VERIZONA PUBLISHER
Publishing Your Ideas

www.verizonaonlinepublishing.com
Vol: 2, Issue: 1

Journal of Robotics and Mechanical Engineering Research

Neural Network based Shape Recovery from SEM Images Using Secondary Electron Image and Reflecting Electron Image

Hiroyasu Usami[1], Yuji Iwahori[1*], Yoshinori Adachi[2], Robert J. Woodham[3], Aili Wang[4] and Boonserm Kijsirikul[5]

[1]Dept. of Computer Science, Chubu University, Kasugai 487-8501, Japan

[2]Dept. of Business Admin. Chubu University, Kasugai 487-8501, Japan

[3]Dept. of Computer Science, University of British Columbia, Vancouver B.C., Canada V6T 1Z4

[4]Dept. of Comm. Eng. Harbin Univ. of Sci. and Tech. Harbin, China

[5]Dept. of Computer Eng. Chulalongkorn University, Bangkok, Thailand

***Corresponding author:** Yuji Iwahori, Dept. of Computer Science, Chubu University, Kasugai 487-8501, Japan; E mail: iwahori@cs.chubu.ac.jp

Article Type: Research, **Submission Date**: 10 July 2017, **Accepted Date:** 28 July 2017 2017, **Published Date:** 04 September 2017.

Citation: Hiroyasu Usami, Yuji Iwahori, Yoshinori Adachi, Robert J. Woodham, Aili Wang and Boonserm Kijsirikul (2017) Neural Network based Shape Recovery from SEM Images Using Secondary Electron Image and Reflecting Electron Image. J Robot Mech Eng Resr 2(1): 7-17. doi: https://doi.org/10.24218/jrmer.2017.22.

Abstract

Scanning Electron Microscope (SEM) is used to see some object with micro size and shape. Although SEM has been a popular measuring equipment, some limitation exists to recover the 3D shape of an object with complicated shape especially for an object with some convex and concave shape. SEM uses the secondary electron microscope in general but some SEM can use the reflecting electron to see the object image further. When the second electron image is used to recover the shape, only one image is available to recover the shape. However, there are some limitations to recover the shape in general. So this paperproposes a neural network based approach to recover 3D shape of an object with some complicated shape including the object without any texture information using not only the secondary electron image but also the reflecting electron image. Experiments are demonstrated with these SEM images to evaluate the validity of proposed approach.

Introduction

It is an important issue to develop a new approach to recover the 3D information of a target object in the field of computer vision. Human uses many queues to estimate 3D information from 2D image(s) including stereo vision using edge or color information in real time. However, implementation in a computer system has some problem to recover the 3D shape of an object since computer system can estimate 3D information using some assumption for the target object in general.

There are some representative approaches in computer vision for this purpose but sometimes conditions or assumptions are limited to apply the approach and these are based on the environment and its purpose. This means that general approach which is useful to some specific approach does not exist. Computer vision based approaches consist of two kinds of approaches in general, one of which uses stereo vision [1] or multiple cameras are used, while the other uses Shape- from-shading or photometric stereo approach [2]. Stereo vision estimates the depth map using disparity of two cameras, while photometric approach estimates the surface orientation (further depth map) from multiple images taken by changing lighting source directions under a fixed camera.

Original SFS and photometric approach uses the assumption that the object has Lambertian reflectance and that light source directions are treated as known parameters. However most objects do not have Lambertian reflectance and this assumption becomes sometimes problem to recover the exact shape.

Scanning Electron Microscope (SEM) image is not Lambertian image and it is usually taken as the secondary electron image when some test object is observed. Practical applications of 3D recovery technology based on SEM are used for shape evaluation of semiconductor devices, steel plate surface and so on. Some environment of SEM consists of using only the secondary electron image. In this case, only one image is available to observe the test image and to recover the shape. There are some methods to recover the 3D shape by solving Eikonal equation [3] and to recover the Eikonal equation faster without calculation of convergence by applying Fast Marching Method (FMM) [4] to shape-from-shading problem [5]. These methods use only one image taken under the condition that parallel light source and parallel projection are used. Although this FMM solves the depth Z from the near to far toward the surrounding points starting from the initial point which is usually specified as the darkest point if the secondary electron image is assumed. Tankus [6] and Yuen [7] tried to extend FMM to the condition of perspective projection to derive more accurate depth map [8]. The problem is it is still difficult to recover 3D shape of test objects with convex and concave curvatures.

Although there is some limitations for 3D shape recovery from only one secondary electron image, there are some possibility to use more images where SEM [9] can utilize the reflecting images except the secondary electron image and these reflection images are observed as the additional images obtained by the reflecting image sensors in SEM.

Authors have developed an approach to recover 3D shape of test objects from SEM image using optimization of Hopfield Neural Network [10]. This method uses three images observed under the tilt of ±10 degrees with tilted table and solves the surface gradient parameters and the depth using the global optimization with the smoothness constraint.

Another paper introduces an approach using FMM [11] and proposed modification of observed SEM image using affine transform [12]. This paper does not assume some specific reflectance function instead Neural Network can learn the mapping between surface gradient and image intensity using actual SEM image. When the direction of light source (exactly not the light source but the direction of secondary electron beam) is an oblique direction, obtained shape becomes the incorrect one but the paper modifies the original image so that FMM can be applied properly under the condition of the frontal direction (of beam direction). However, this approach [12] is based on FMM and it is applicable to the monotonically convex object and further extension is necessary to apply the method to the convex and concave surface. SEM hard- ware environment has been widely extended according to the progress of special surface processing and nano technologies [13-15] and more flexible approach is expected to recover the convex and concave surface from SEM images.

Another paper [16] recovers surface gradients using shape-from-shading approach using reflecting electron images. This paper treats two images for the relatively simple shape and it may be difficult to recover the 3D shape for the convex and concave curved surface with a complicated shape.

This paper proposes a specific approach to recover the 3D shape of the target object which is observed using the Scanning Electron Microscope (SEM). Both sphere and test object are processed with the same coating to perform the same reflectance property. SEM images consist of different kind of image, where the original image is the secondary electron image and other three kinds of reflecting electron images are available in observation. These four images observed at the different conditions can be used to recover the 3D shape if some characteristics of SEM environment are commonly used. Here, photometric stereo based approach is a good choice to solve the problem using reflecting electron images except the secondary electron image. First, the approach learns the input/output mapping using neural network. The paper shows the learned neural network can then be applied to each point of test object to obtain the surface gradient of each point. Integrating the surface orientation can recover the 3D shape of the height map.

Computer simulation is applied for the proposed approach, where the error is evaluated for the proposed approach. Real images are also used for the demonstration of the proposed approach in the experiments. It is shown that the approach is useful for the convex and concave object and the proposed approach provides the better result than that of the previous approach.

Principle of SEM Image

Observation System of SEM

The architecture of the SEM is shown in Figure 1. SEM image has the following properties.

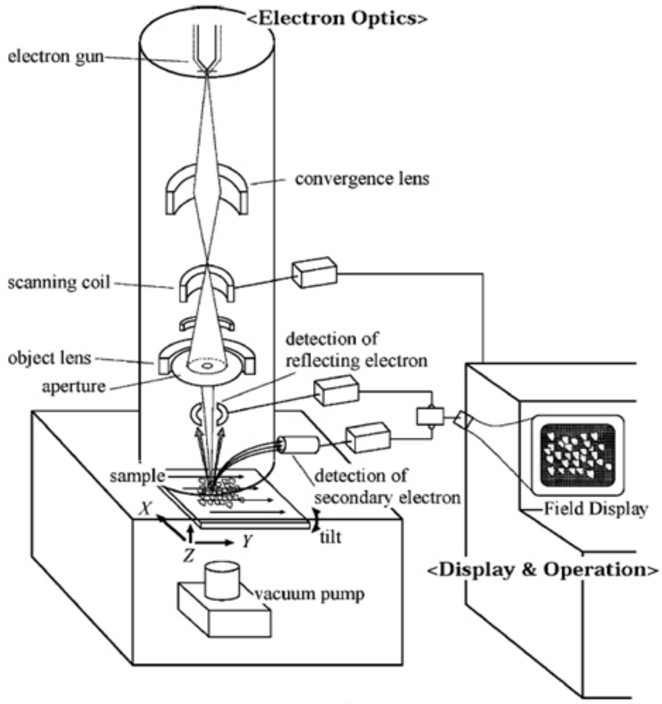

Figure 1: Scanning Electron Microscope

a). The brightness becomes low for the point that the surface normal is toward the viewing direction.

a). The light source and the viewing point is assumed to be located at the same position.

a). Cast shadow does not occur.

Projection of SEM

SEM has 4 kinds of electron sensors to detect the electrons.

Although whole SEM images are available in any SEM environment, some combination of these electron images may produce several kinds of images. Projection consists of mainly two kinds. Here, SEM image produced by each projection is explained.

Secondary Electron Image: Scanning the irradiated electron beam on the surface of the charged test sample and measuring the amount of secondary electrons generated by ejecting the charged electrons provides the output image called SEI (Secondary Electron Image). An example of SEI is shown in Figure 2.

As shown in Figure 2, SEI is observed as an inverse image to the normal shading image illuminated by the parallel light, and the darkest point corresponds to the brightest point of the normal shading image. Secondary electron generated from a test sample is converted into electron signals by a photomultiplier.

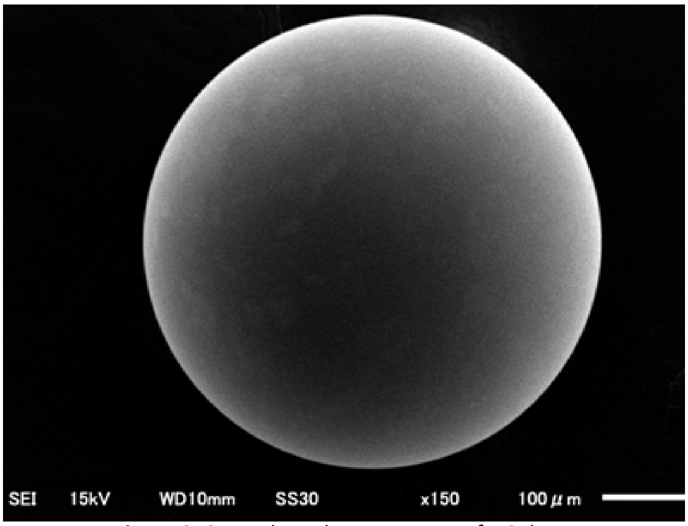

Figure 2: Secondary Electron Image of a Sphere

Secondary electrons emitted from the shadowed surface are captured by the detector for observing the secondary electrons. As a feature of the secondary electron image, a shadow less image can be obtained as shown in Figure 3. The resulting image is similar as that obtained by the original light source and reflector as shown in the right figure of Figure 4.

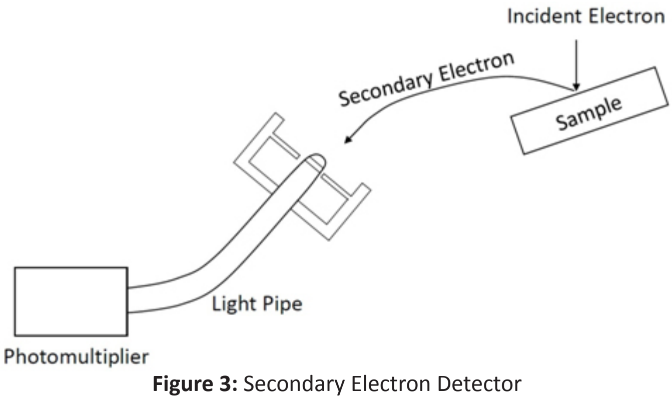

Figure 3: Secondary Electron Detector

Projection of Reflecting Electron: Reflecting electron is obtained by scanning the irradiated electron beam onto the test sample and by reflecting (backscattering) on the test sample. Reflecting electron is observed by three detectors and output as images. Figure 5 is a backscattered electron observation sys- tem. Figure 5 shows three detectors which consist of reflecting electron detectors A and B arranged evenly on the left and right, and reflecting electron detector C arranged at another angle.

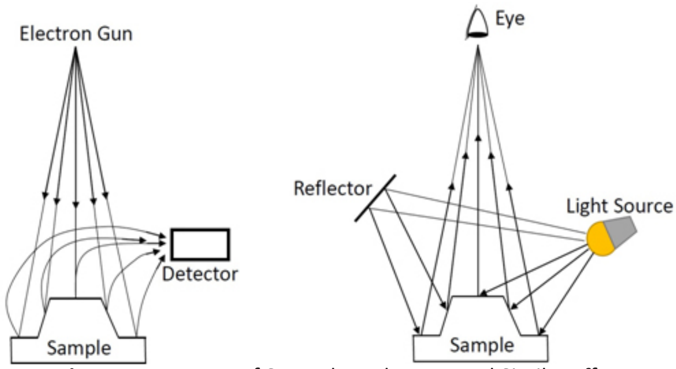

Figure 4: Detector of Secondary Electron and Similar Effect

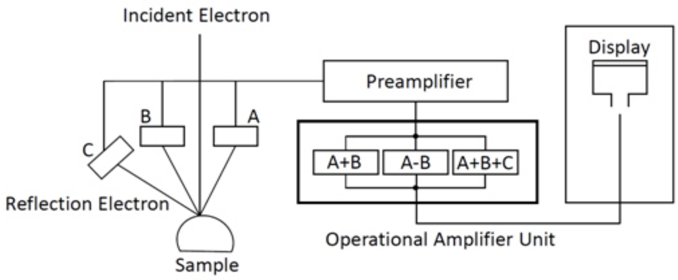

Figure 5: Detector of Reflecting Electron

The signal observed by the detector is amplified by the preamplifier and calculation of each signal is performed. Three kinds of different images can be output through this calculation by performing three operations on the signal obtained from the detector. Features of each image and how to extract the signals are described next.

BEIC Image: BEIC image can be generated just like that illuminated from the frontal direction. This BEIC image is obtained by extracting the sum of the signal of detector A and the signal of B (See Figure 6).

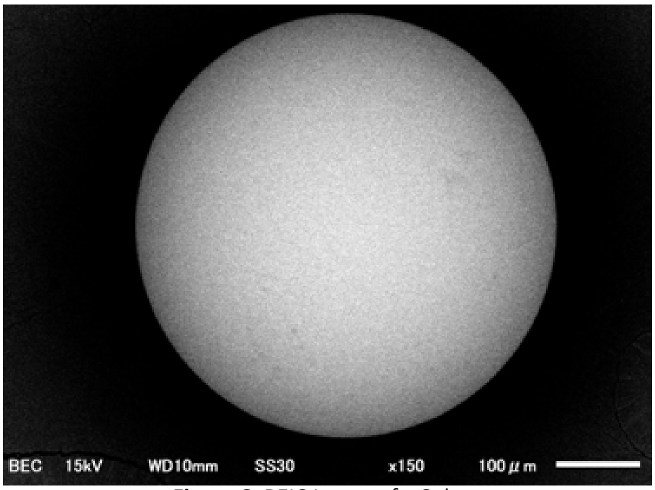

Figure 6: BEIC Image of a Sphere

BEIT Image: BEIT image can be generated just like that illuminated from the right direction. This BEIT image is obtained by extracting the difference between the signal of detector A and the signal of B (See Figure 7).

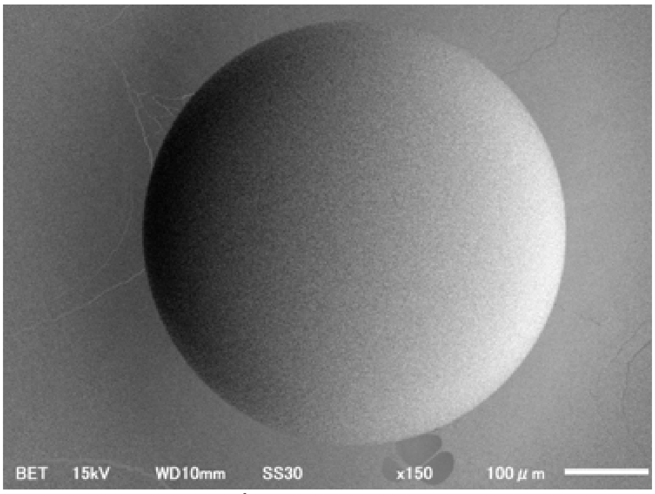

Figure 7: BEIT Image

BEIS Image: BEIS image is a combined image which the composition information of the test sample surface and the convex/concave information are mixed. This BEIS image is obtained by extracting the sum of the signals of all the detectors A, B, C (See Figure 8).

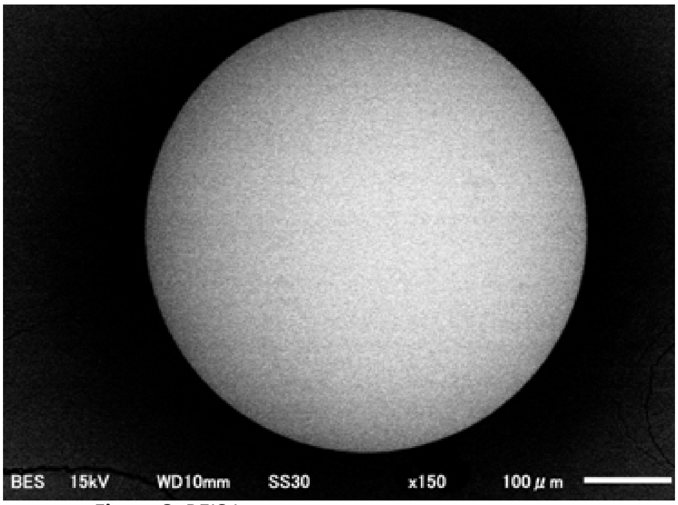

Figure 8: BEIS Image

Obtaining 3D Shape from SEM Images

Neural Network Based Photometric Stereo

Paper [12] recovers 3D shape of a test sample from SEI (image). FMM set an initial depth Z at the nearest point from the view point to a monotonic convex object and solves the depth Z towards the surrounding points. FMM uses only one image and problem is that FMM cannot be applied directly to the convex/concave surface.

Paper [16] recovers surface gradient parameters from shading information using the signals obtained from each detector of A and B. Interesting observation is the approach uses two reflecting electron images and it is applied to the monotonic convex object based on the idea of two light source approach. The method has not applied to the complicated shape and it is considered that some limitation still exists based on the assumption of the approaches.

This paper proposes a further approach to recover the 3D shape from multiple images obtained through SEM using Neural Network based Photometric Stereo. The proposed approach can be applied to a complex shape and surface gradient parameters are obtained locally using both of a sphere and a test sample images.

The implementation of Neural Network to Photometric Stereo is proposed in paper [17] by main authors originally and this paper is the first paper which extends this Neural Network based Photometric Stereo to the SEM world problem.

Neural Network learns the mapping between multiple image intensity as input and the corresponding gradient parameters as output using various points on a sphere. This paper introduces this original idea and applies to the SEM problem. No specific assumption has been made for the surface reflectance function nor light source directions since the method is still available as far as the surface reflectance properties and light sources are the same between a sphere and a test sample even if SEM image is applied. Coating processing is sometimes used to observe a test sample and this processing is also applied before taking SEM images to realize the same reflectance properties between a sphere and a test sample.

A sphere has the various points which have different surface gradient uniformly on the object. Taking sample points and learning these points can provide the sufficient learning using a neural network. LUT (Look Up Table) is another solution but some interpolation is necessary in the implementation of LUT, instead NN has an advantage to interpolate the mapping of input and output with multiple dimensional space.

NN Learning is done using 4 SEM images (SEI, BEIT, BEIC, BEIS) of a sphere. Input of NN is given as the vector (E_1, E_2, E_3, E_4) which corresponds to the normalized image intensity between 0 and 1, while output of NN is given as the corresponding surface gradient vector (Nx, Ny, Nz) ofthe sphere. Radial Basis Function Neural Network (RBF-NN) is used to learn the mapping since RBF-NN can treat the many learning data with high dimensions. RBF-NN can perform multidimensional non-linear functional approximation via the learning for a sphere and estimate the corresponding surface gradient vector $\boldsymbol{n}$, i.e., (Nx, Ny, Nz) in the generalization after the learning for a given input (E_1, E_2, E_3, E_4) of an each point of a test sample.

Learning procedure using RBF-NN for sphere images are shown in Figure 9. The mapping between input and the corresponding output is learned by this RBF-NN using many sample points on a sphere.

Learned RBF-NN is used for the generalization of a test sample. Similarly 4 image of a test sample is used in input, then the corresponding output is obtained using learned RBF- NN. Thus surface gradient vector is obtained at each point of a test sample and this output is used to recover the 3D shape.

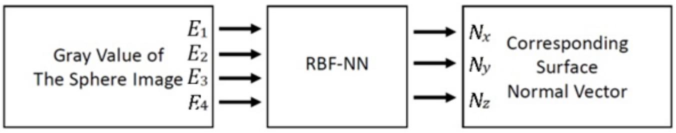

Figure 9: Learning Procedure of RBF-NN

RBF-NN Functional Approximation: Neural networks are attractive for non-parametric functional approximation. A radial basis function (RBF) neural network is one choice suitable for many applications. In particular, it has beenwidely used for strict interpolation in multidimensional spaces. It is argued that RBF neural networks often can be designed in a fraction of the time it takes to train standard feed-forward networks. They are claimed to work well when many training vectors are available.

RBF networks represent non-linearity via the choice of basic functions. A Gaussian isn't the only choice of radial basis function for RBF networks but it is the choice widely used and the one used here. One common learning algorithm for RBF networks is based on first randomly choosing data points as RBF centers and then solving for the optimal weights of the network. Performance, however, critically depends on the chosen centers. In practice the centers often are chosen to be an arbitrarily selected subset of the data points. This selection mechanism typically is unsatisfactory. The resulting network may perform poorly, because the centers do not suitably sample the input data, or it may have excessive size, if a very large number of centers is used.

An alternative learning procedure is based on an orthogonal least squares (OLS) method [17]. Of course, the performance of an RBF network still critically depends on the chosen cen- ters. Because a fixed center corresponds to a given regressor in a given regression model, the selection of RBF centers can be regarded as a problem of subset model selection. The OLS method can be employed as a forward regression procedure to select a suitable set of centers (regressors) from a large set of candidates. At each step of the regression, the increment to the explained variance of the desired output is maximized.

The learning procedure adopted here is based on the above orthogonal least squares learning method. It chooses radial basis function centers one by one in a systematic way until an adequate network has been constructed. The algorithm has the property that each selected center maximizes the increment to the explained variance of the desired output while remaining numerically well-conditioned.

The learning procedure builds an RBF neural network one neuron at a time. Neurons are added to the network until the sum-squared error falls beneath an error goal (or a maximum number of neurons have been used). In learning, it isimportant that the so-called spread constant of the radial basis function be large enough that the neurons respond to overlapping regions of the input space, but not so large that all the neurons respond in essentially the same manner. Once learning is complete, that which has been learned is represented by the weights connecting each RBF neural network unit. The resulting network generalizes in that it predicts a surface normal, [*Nx*, *Ny*, *Nz*], given any triple of input values, [E_1, E_2, E_3, E_4]. The resulting network trained using the calibration sphere can then be used to estimate the surface orientation of other test objects.

The architecture of RBF-NN used in this paper is shown in Figure 10. Here, (E_1, E_2, E_3, E_4) represents 4 input image intensities as input, and (*Nx*, *Ny*, *Nz*) represents 3 output component of surface gradients as a unit vector. *w* represents the weights, *n* represents the output of convolution, *a* represents the output of RBF, and *b* represents the threshold when convolution processing is applied in RBF-NN.

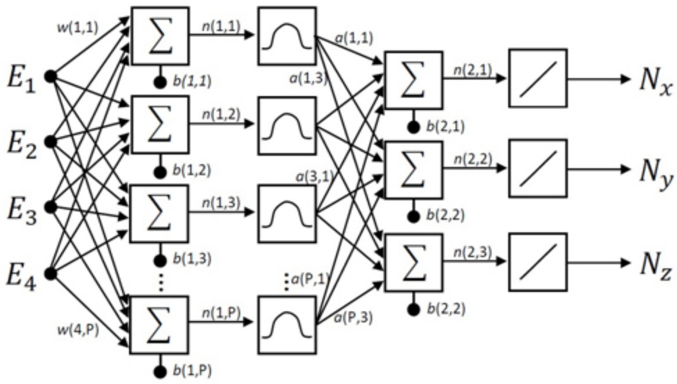

Figure 10: Architecture of RBF-NN

Surface Gradient Parameters: The surface gradient vector is obtained as ($N'x$, $N'y$, $N'z$) and the surface gradient parameters $(p,q)=(,)$ are given as follows

$$p = -\frac{N_x}{N_y}, q = -\frac{N_y}{N_z} \tag{1}$$

Gradient parameters (*p*, *q*) are integrated along the *X* and *Y* direction, respectively to obtain the height distribution *Z*. The proposed approach can be applied to convex/concave surface of a test sample. This is an advantage for that FMM cannot be applied to recover the complicated shape.

Eq.(1) takes very big value for *p* or *q* and Median Filter and Gaussian Filter are applied to the whole results of (*p*, *q*) at all points obtained by this approach to obtain the smooth height distribution of *Z*.

Recovery of Height Distribution

Using the obtained (*p*, *q*), the proposed approach recovers the height *Z* distribution. Recovering *Z* is done for the object region which is made as a mask image. Let ***Known*** points be the points where the calculation of *Z* is done, let ***Unknown*** points where the calculation of *Z* is still remained and let ***Look*** point be the reference point. Procedures to calculate the depth *Z* are explained here.

Step1. Initial point is set to the point which is the nearest point from the gravity center and this initial point is represented as ***Known*** point.

Step2. The depth Z is calculated for each of four neighbor- ing points of the initial point using (p,q) and these points are set to be ***Known*** points.

Step3. When some ***Unknown*** point exists with more than two known points around its 8 neighboring points, the point is set to be candidate of ***Look*** point.

Step4. Z of ***Look*** point is calculated from the mean of integral from each of two points among four neigh- boring points, then this point is labelled as ***Known*** point.

Step5. Repeat Step3 to Step4 until there are no ***Unknown*** points.

Setting Initial Point: It is necessary to set an initial point to calculate Z distribution. The initial point is set as follows. Gravity center of mask region of a test sample is obtained as shown in Figure 11(b). To avoid the case when the gravity center is out of the mask region, skeleton image is derived and its gravity center is calculated as shown in Figure 12(a). Gravity center point and skeleton image are shown in Figure 12(b). Nearest point to the gravity center point on the skeleton is obtained and the point is set as an initial point. Skeleton image with its initial point is shown in Figure 13.

Calculating Height Z: Z at the initial point is set to be 0 and integration of (p, q) is applied to obtain Z distribution. p along X and q along Y is added or subtracted from the initial point and Figure 14 shows the integration of the surface gradient parameters (p, q). When Z is known at some point, integration is applied for 8 neighbor points sequentially.

(a) Example of Mask Image (b) Gravity Center of Mask Region

Figure 11: Setting of Mask1

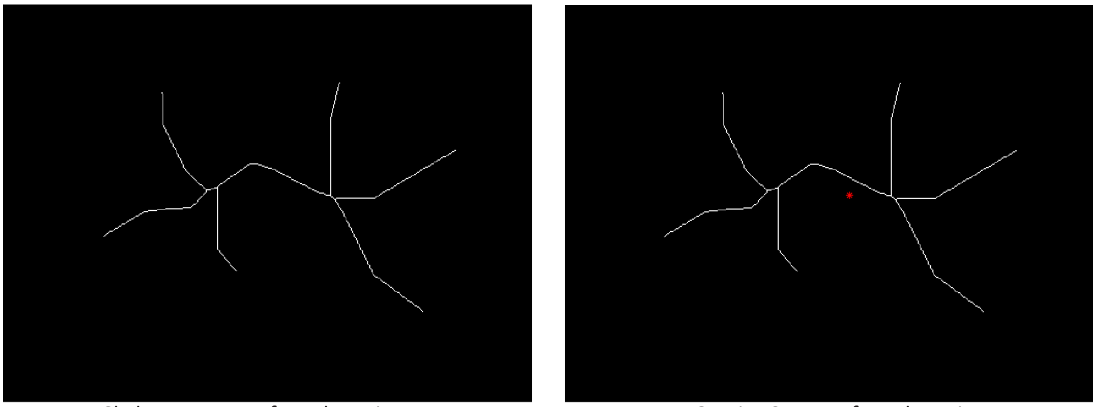

Skeleton Image of Mask Region Gravity Center of Mask Region

Figure 12: Setting of Mask 2

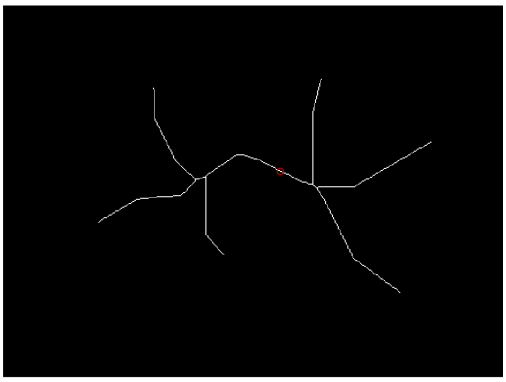

Figure 13: Initial Point

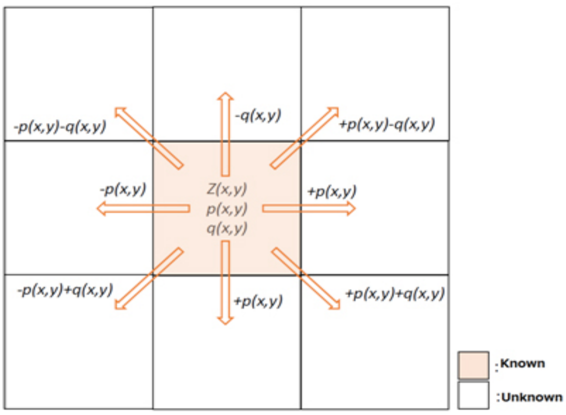

Figure 14: Integral Operation

Taking mean value of integral operations from two points can reduce the error for X and Y to improve the accuracy of Z. In the initial stage, four neighboring points around the initial point are calculated since the initial point is just one point. After that, interesting points ***Look*** are taken as point which has more than two ***Known*** points among 8 neighboring points. Z is calculated for ***Unknown*** point when more than two points exist among 8 neighboring points. When more than three ***Known*** points exists among 8 neighboring points of the interesting point, four neighboring points are calculated with higher priority and two points are selected as shown in Figure 15.

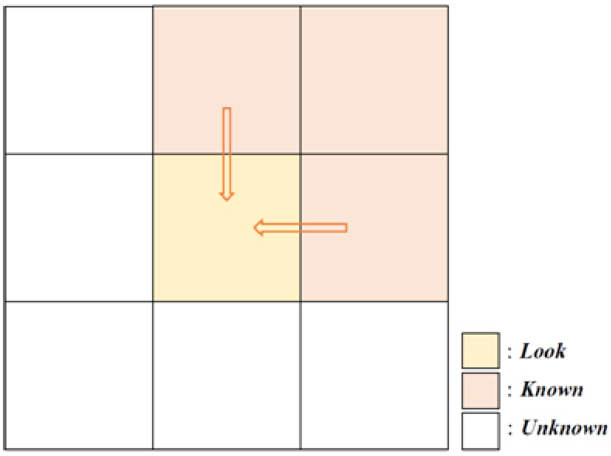

Figure 15: Four Neighboring Points with Higher Priority

Either of p or q is used to calculate Z at four neighboring points but both of p and q are used to calculate Z at 8 neighboring points. Another process is applied when more than two points exist among 8 neighboring points to reduce the reference of oblique points. Integral processing is repeated until there are no ***Unknown*** points in the mask region.

Experiments

The proposed approach is evaluated in the experiments. SEM images are taken and used to recover the 3D shape, where HITACHI S-3500N is used to take the observed SEM images. Specification of this SEM are shown in Table 1.

Table 1: Specification of SEM

Name	**SEMHITACHI S-3500N**
Resolution	3.0nm
Accelerating voltage	0.5-30kV
Observation magnification	×15-×200000
Maximum Size of TestSample	150mm

Four images are taken for a sphere and a test sample, respectively. SEM image itself has some noise and multiple images are taken and arithmetic mean were used to increase the accuracy. Degree of reducing noise is shown in Figure 16.

Figure16 shows that noise was reduced by taking the arithmetic mean.

Each input image of SEM (SEI, BEIC, BEIT and BEIS) is normalized between 0 and 1 so that dynamic range takes the same range.

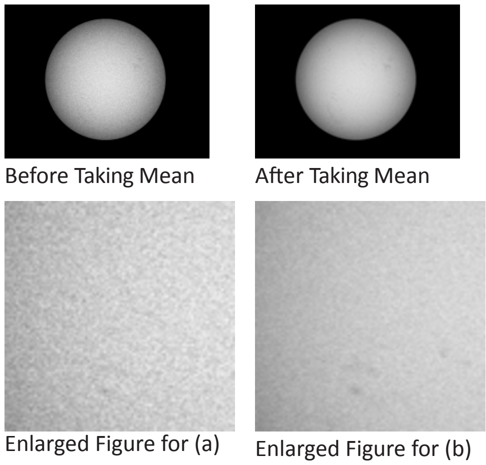

Figure 16: Noise Reduction by Arithmetic Mean

Image resolution taken under SEM environment is 2560 ×1920. Here, resolution of sphere images was taken to be 1024×768 and that of test sample was taken to be 512×384. This to perform the effective learning and the effective output of results.

Slope and *Aspect* were used for the visualization of surface gradients distribution. *Slope* represents the visualization of angles between the surface normal vector and viewing direction vector. *Aspect* represents the directional component at each point with a short line segment.

Slope and *Aspect* are viewpoint dependent measures and equations of *Slope* and *Aspect* are shown below.

$$Slope = \tan^{-1}\sqrt{p^2+q^2} \tag{2}$$

$$Aspect = \tan^{-1}\frac{p}{q} \tag{3}$$

Evaluation of Accuracy

Sphere images with radius 0.25mm are taken by SEM and used for the NN learning. Here the accuracy is evaluated for the sphere by obtaining surface gradient vector. Four images are given as input of NN and corresponding surface normal vector is given as output of NN. Number of sampled points used for the learning was 71765, number of maximum learning epochs was 300, and goal was set to 0.001. Spread parameter of Radial Basis Function was set to 0.3. Figure 17 shows the status of the NN learning and Figure 18 shows input images of a sphere used in this experiment respectively.

Results: Obtained *Slope* and *Aspect* for a sphere of Figure 18 are compared with that of the ground truth and the results are shown in Figure 19. Location of initial point and the result of the true height and obtained height are compared in Figure 20.

It is shown that close results to the true shape are obtained through Figure 19 and Figure 20. Next proposed approach was evaluated with accuracy.

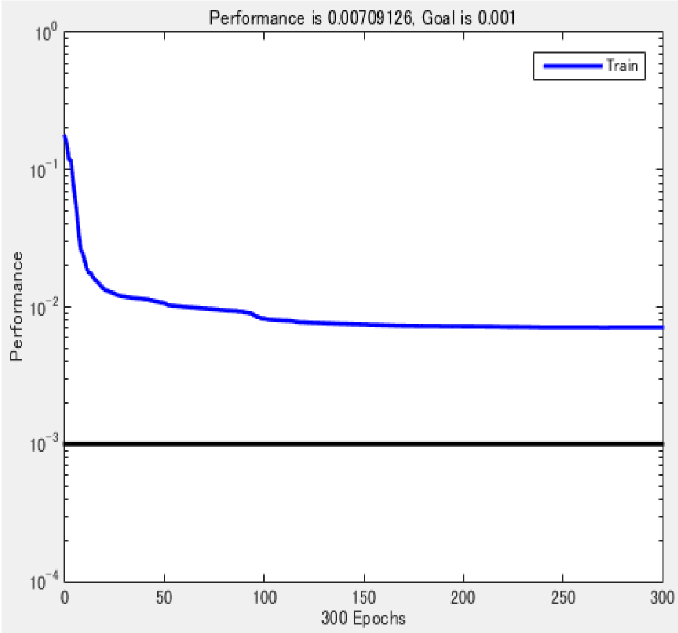

Figure 17: Learning Status

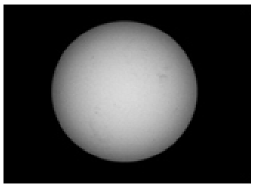

(a) BEIC Image

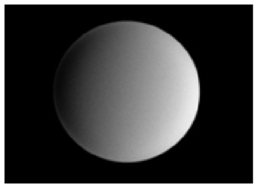

(b) BEIT Image

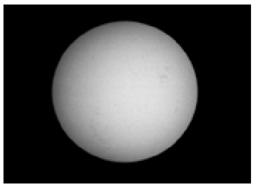

(c)BEIS Image

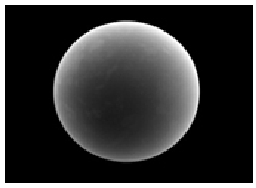

(d) SEI Image

Figure 18: Input Images for NN Learning

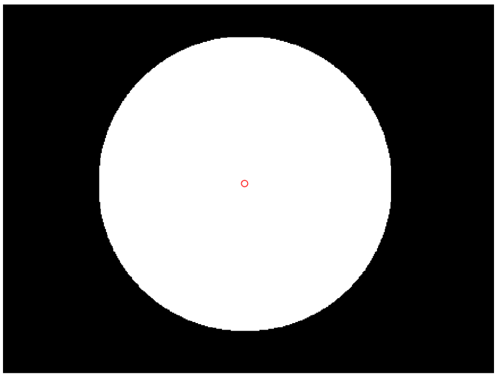

Position of Initial Point

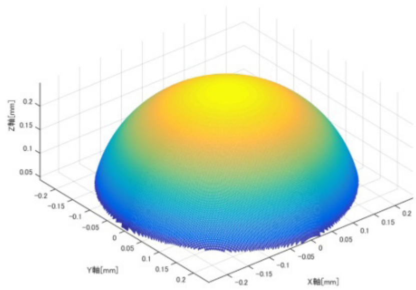

True *Z*

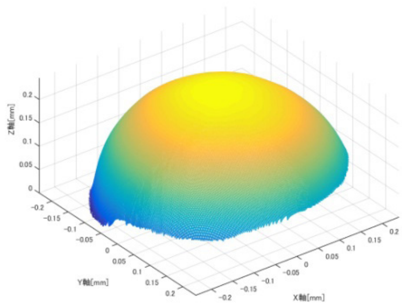

Obtained *Z*

Figure 20: Comparison with True Height

Evaluation of Accuracy: The accuracy of Z was evaluated for the result obtained by the proposed approach. Degree error of surface gradient vector was used for the evaluation. Number of points for comparison, mean error of degree and mean error of *Z* are shown in Table 2.

It is shown that error is within 4 % for the whole points of a sphere and NN produced acceptable results for the shape.

Generalization of NN to Test Sample: Images shown in Figure 18 are used for the learning and generalization of NN was performed to another test sample object.

Table 2: Evaluation of Error

	Proposed Approach
Number of points forcomparison	71765 points
Mean Error of Degree	5.8017 deg.
Mean Error ofZ	0.0112mm

Test sample images are taken under the same condition using SEM after taking sphere images. Coating processing is applied for both of a sphere and a test sample. Learning is done for a sphere images and after the NN learning, NN is used for the generalization to another test sample and 3D shape was obtained using the learned NN. Parameters for NN learning are given as the same parameters when a sphere is learned with this RBF-NN.

Four images taken for the ant's compound eye with multiple convex shape are shown in Figure 21. Further images of hair root and other handmade objects by solder are shown in Figure 22, Figure 23 and Figure 24, respectively.

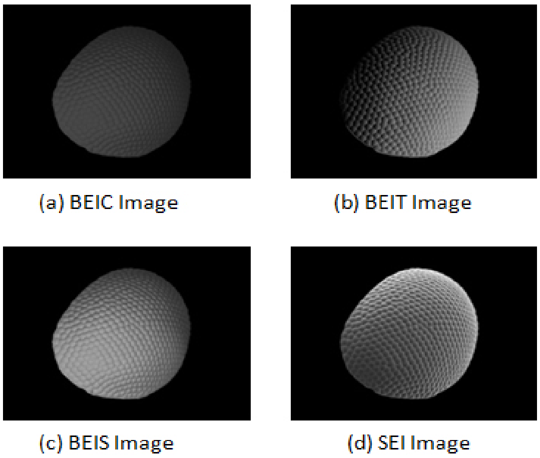

Figure 21: Input Images of Ant's Compound Eye

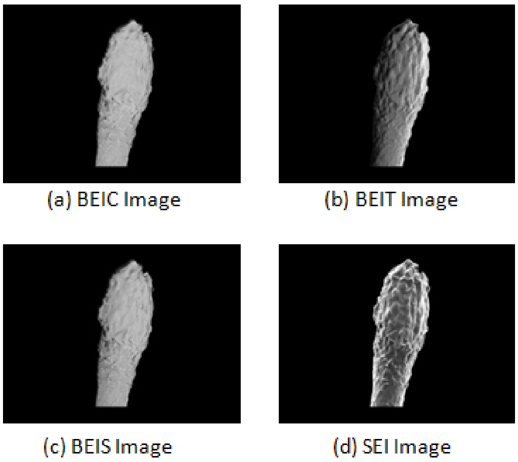

Figure 22: Input Images of Hair Root

Results: Height distribution of Z was obtained by in- tegrating (p, q) obtained from each input images of Figure 21, Figure 22, Figure 23 and Figure 24, respectively. Results of *Slope*, *Aspect* and Z are shown in Figure 25, Figure 26, Figure 27 and Figure 28, respectively. Results by the approach [12] are shown for the comparison. Since the approach [12] should take the initial point at the highest point and the location of this initial point taken in the approach [12] is also shown.

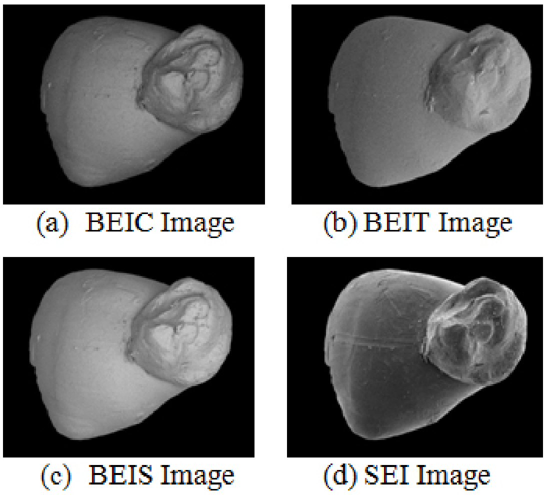

Figure 23: Input Images of Solder 1

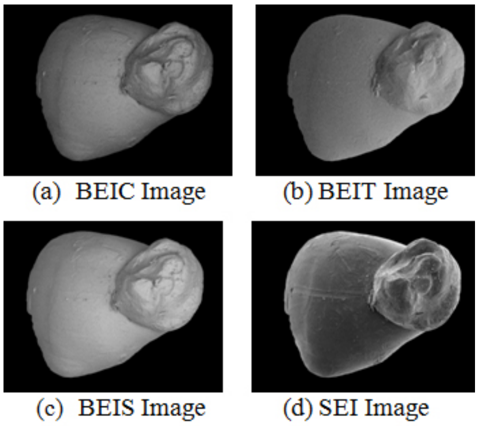

Figure 24: Input Images of Solder 2

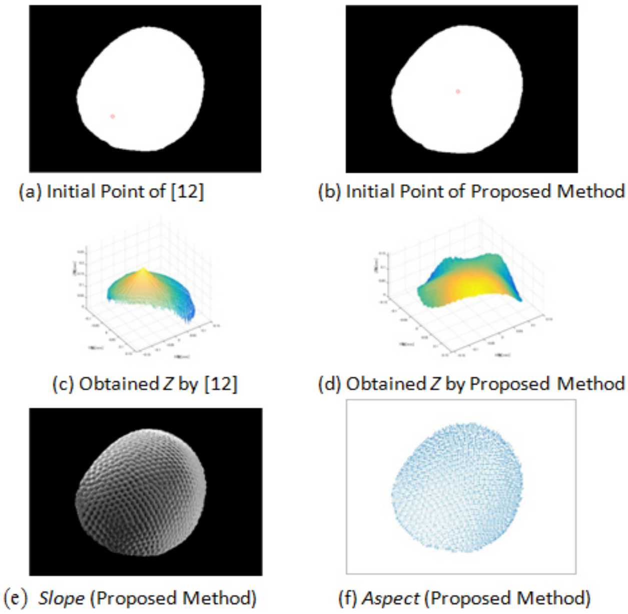

Figure 25: Results of Ant's Compound Eye

FMM takes the highest point of Z as an initial point and recovers from high to low points. This method gives acceptable results for monotonic convex shape with one highest point as shown in Figure 26 or Figure 27. However, it is difficult to specify the highest point in general from SEM images since size of object is too small. While the proposed method uses some initial point in the mask region of object and the initial point is automatically determined and Z is recovered.

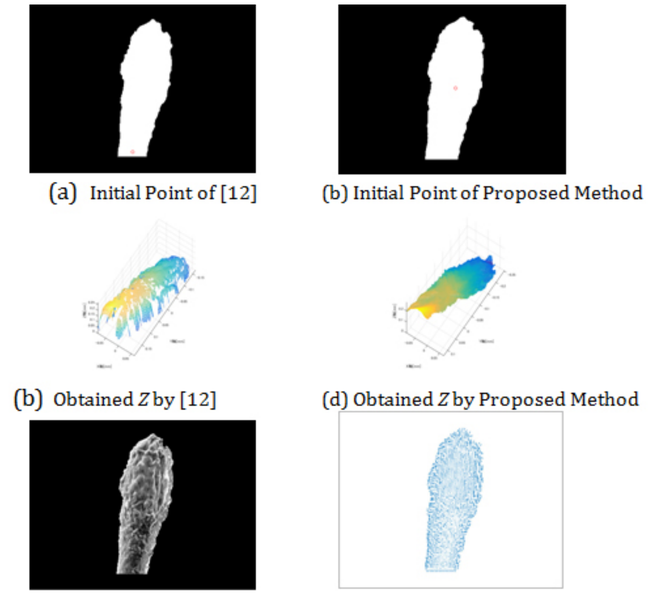

(a) Initial Point of [12] (b) Initial Point of Proposed Method

(b) Obtained *Z* by [12] (d) Obtained *Z* by Proposed Method

(e) *Slope* (Proposed Method) (f) *Aspect* (Proposed Method)

Figure 26: Results of Hair Root

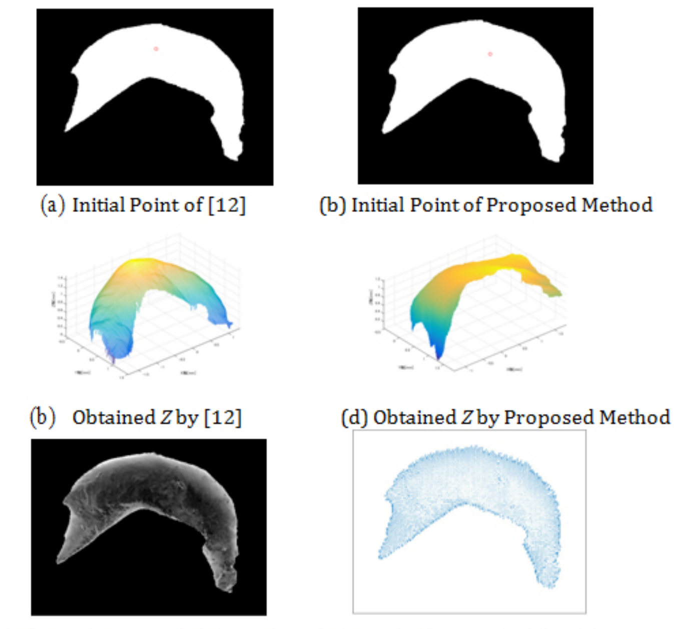

(a) Initial Point of [12] (b) Initial Point of Proposed Method

(b) Obtained *Z* by [12] (d) Obtained *Z* by Proposed Method

(e) *Slope* (Proposed Method) (f) *Aspect* (Proposed Method)

Figure 27: Results of Solder 1

Method [12] cannot be applied for test sample with more than two high points as shown in Figure 25 or Figure 28 in general, while the proposed method gives acceptable results with the convex and concave shape. Thus it is shown that proposed method uses multiple SEM images and gives robust results for shape recovery.

No assumptions are used for surface reflectance by taking the same coating processing for both of a sphere and a test sample. The method also has advantage that the dense recovery is performed for each point of a test sample. Through these observations, the proposed method is effective and gives acceptable results for 3D shape recovery from SEM images.

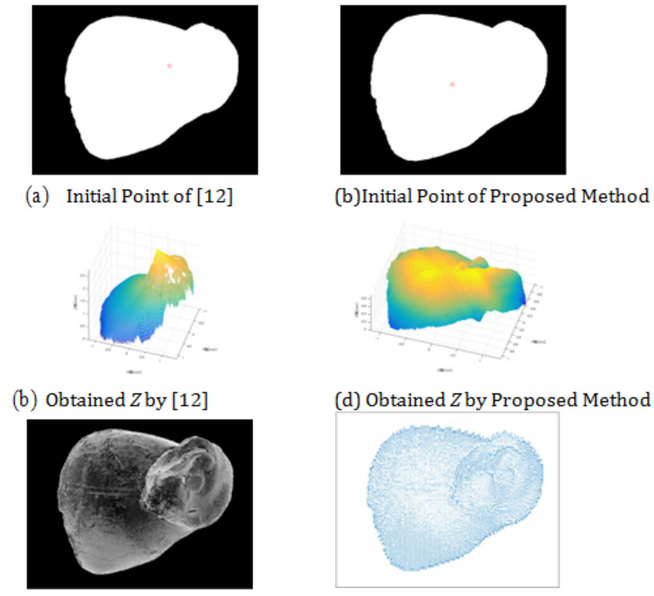

(a) Initial Point of [12] (b)Initial Point of Proposed Method

(b) Obtained *Z* by [12] (d) Obtained *Z* by Proposed Method

(d) *Slope*(Proposed Method) (f) *Aspect* (Proposed Method)

Figure 28: Results of Solder 2

Conclusion

This paper proposed a new approach to apply the NN based photometric stereo to the problem to recover 3D shape from SEM images. The paper shows that four different images consisting of three kinds of reflecting electron image (BEIC, BEIT, BEIS) and one secondary electron image (SEI) can be used for NN learning and generalization. The surface gradient vector is obtained from the output of NN and integrating the surface gradient parameters gives the height distribution as a recovered shape.

The paper showed NN learning using a sphere was effectively done and generalization of the learned NN to another test sample gives acceptable shape. RBF-NN is effectively used to recover the shape.

SEM images have some noise and the approach reduced the effect of noise by taking arithmetic mean and normalization of intensity range was also applied for the NN learning to increase the accuracy of surface gradients.

Learning was done the higher resolution image of a sphere. This enables to take higher accuracy for the output of a test sample.

Surface gradient parameters were obtained by *Slope* and *Aspect*. The experiment gave the mean error for the surface gradients gave the error within 4%. The proposed method was compared with the previous FMM based approach and it was shown that the method gives the better results. It is also shown that the approach is available for not only monotonic convex object but also complicated surface with convex/concave shape.

Further effort to reduce noise effect to the obtained SEM images is remained to improve better results or some extension of this approach with stereo vision approach is remained as future subjects.

Acknowledgement

Iwahori's research is supported by Japan Society for the Promotion of Science (JSPS) Grant-in-Aid Scientific Research (C) (17K00252) and Chubu University Grant. The authors also thank Naoya Iwamoto of the lab for his experimental help and thank lab member for their useful discussions.

References

1. Ojima H, Murakami Y, Otsuka H, Sasamoto Y, ZhouL, Shimizu J, et al. 3D Data Acquisition and Reconstruction from SEM Stereo Pairs. Journal of the Japan Society for Precision Engineering. 2009; 75(6):773-777.
2. Horn BKP, Brooks MJ. Shape from Shading. The MIT Press; 1989.
3. Verbeek PW, Verwer BJH. Shading from shape, the eikonal equation solved by gray-weighted distance transform. Pattern Recog- nition Letters. 1990; 11:681–690.
4. James A. Sethian. A Fast Marching Level Set Method for Monotonically Advancing Fronts. Proceedings of the National Academy of Sciences of the United States of America (PNAS U. S.). 1996; 93(4):1591–1593.
5. Kimmel R, Sethian JA. Optimal Algorithm for Shape from Shading and Path Planning.JMIV. 2001;14:237-244.
6. Tankus A, Sochen N, Yeshurun Y. Shape-from-Shading under Perspective Projection. IJCV. 2005; 63(1):21-43.
7. Yuen SY, Tsui YY, Chow CK. A Fast Marching Formulation of Perspective Shape from Shading under Frontal Illumination. Pattern Recognition Letters. 2007; 28:806-824.
8. Kimmel R, Sethian JA. Optimal Algorithm for Shape from Shading and Path Planning. Journal of Mathematical Imaging and Vision (JMIV). 2001; 14(3)237–244.
9. Jiang J, x Sakai J. 3-Dimensional Measurement of Fracture Surface Using SEM via the Combination of Stereo Matching and Integrating Secondary Electron Intensity. Journal of the Japan Society of Mechanical Engineers. 2002; 68(666):120-126.
10. Iwahori Y, Kawanaka H, Fukui H, Funahashi K. Obtaining Shape from Scanning Electron Microscope using Hopfield Neural Network. Journal of Intelligent Manufacturing. 2005; 16(6):715-725.
11. Iwahori Y, Shibata K, Kawanaka H, Funahashi K, Woodham RJ, Adachi Y. Obtaining Shape from SEM Image Using Intensity Modification via Neural Network. Frontiers in Artificial Intelligence and Applications, Advances in Knowledge-Based and Intelligent Information and Engineering Systems. 2012; 243:1778-1787.
12. Iwahori Y, Funahashi K, Woodham RJ, Bhuyan MK. Neural Network Based Image Modification for Shape from Observed SEM Images. IAPR ICPR. 2014:2131-2136.
13. Cameron JA. The use of ultrasonics in the removal of the smear-layer: a scanning electron microscope study. Journal of Endodontics 9.7. 1983:289-292.
14. Haidar Almohri, Chongxiao Du, Zupan Hu, Jingxing Wang. Data Analysis and Prediction of Power Gener- ated by Photovoltaic Systems. Proceedings of the World Congress on Eng and Computer Sci. 2014; 2.
15. Zupan Hu. Contact Around a Sharp Corner with Small Scale Plasticity.Adv.Mater. 2017; 6:10-17.
16. Chen D. A Study on Robust SEM Photometric Stereo Using Two BSE Detectors. Ph.D. Thesis, Hokkaido University; 2014.
17. Iwahori Y, Woodham RJ, Bagheri A. Neural Network Implementation of Photometric Stereo. VisionInterface. 1995:81-88.